Chinese Journal of
POLYMER SCIENCE

RESEARCH ARTICLE

https://doi.org/10.1007/s10118-026-3690-x
Chinese J. Polym. Sci.

Durable Anti-fogging and Abrasion-resistant Coatings Based on Polyoxometalates-Hydrophilic Resin Composites with Enhanced Cohesion and Adhesion

Xu Yang[a], Shu-Di Ying[b], Cong-Cong Zhai[c], Yu-Lin Yin[a], Jian-chao Hou[a], Pan-Pan Zhao[a], Wen-Ting Li[a], Shuai-Jun Yang[a], Jia-Chen Ma[a*], and Xu-Chuan Jiang[a*]

[a] *Institute for Smart Materials & Engineering, School of Materials Science and Engineering, University of Jinan, Jinan 250022, China*
[b] *Huzhou College, Huzhou 313000, China*
[c] *Shandong Institute of Non-Metallic Materials, Jinan 250031, China*

Electronic Supplementary Information

Abstract Achieving long-term anti-fogging performance while maintaining high visible-light transmittance is of critical importance for transparent substrates. However, challenges remain in achieving satisfactory abrasion resistance and weatherability of anti-fogging coatings across different substrates. In this work, an organic-inorganic hybrid anti-fogging coating was developed by integrating a highly adhesive hydrophilic polymer resin with polyoxometalates (POMs). The hydroxyl groups along the polymer chains provide excellent adhesion, while the presence of hydrophilic ionic groups facilitates the rapid formation of a continuous water film upon exposure to water vapor. Moreover, the multiple protons carried by the POMs not only form interfacial bonding with the substrate to further enhance adhesion, but also form multiple hydrogen bonding interactions with the polymer chains to strengthen the coating's cohesion and reduce its surface roughness. As a result, the coating exhibits outstanding abrasion resistance, maintaining excellent anti-fogging performance even after 1200 abrasion cycles under a 500 g load. Furthermore, the strong UV absorption of POMs prevents photoaging of the polymer resin in outdoor environments, imparting remarkable weather resistance. After 240 h of accelerated UV aging (0.68 W/m^2, 60 °C), the coating still delivers effective anti-fogging functionality. This study provides a generalizable strategy for designing environmentally friendly, long-lasting anti-fogging coatings with promising applications in glass, optical devices, and agricultural films.

Keywords Anti-fogging; Superhydrophilic; High abrasion resistance; High weatherability

Citation: Yang, X.; Ying, S. D.; Zhai, C. C.; Yin, Y. L.; Hou, J. C.; Zhao, P. P.; Li, W. T.; Yang, S. J.; Ma, J. C.; Jiang, X. C. Durable anti-fogging and abrasion-resistant coatings based on polyoxometalates-hydrophilic resin composites with enhanced cohesion and adhesion. *Chinese J. Polym. Sci.* https://doi.org/10.1007/s10118-026-3690-x

INTRODUCTION

Transparent substrates such as optical lenses, vehicle windshields, and agricultural greenhouse films possess unique optical properties that endow them with irreplaceable application value.[1–3] However, when the ambient temperature falls below the dew point, water vapor in the air undergoes heterogeneous nucleation and forms discrete microdroplets with diameters of 100–500 nm. Mie scattering from these microdroplets will lead to a sharp decrease in light transmittance, severely compromising the functionality of the transparent substrates.[4] Consequently, various anti-fogging strategies have been developed, including superhydrophobic and superhydrophilic coatings.[5–7]

* Corresponding authors, E-mail: ism_majc@ujn.edu.cn (J.C.M.)
E-mail: ism_jiangxc@ujn.edu.cn (X.C.J.)
Received February 10, 2026; Accepted March 30, 2026; Published online June 10, 2026

Superhydrophobic coatings typically require low-surface-energy materials combined with specific surface roughness to form Cassie structures, which reduce the contact area between droplets and the substrate and enable rapid droplet roll-off. However, this approach suffers from delayed anti-fogging performance under low-humidity conditions, and the fragile micro/nanostructures are easily damaged, leading to loss of anti-fogging functionality.[8–10] In contrast, superhydrophilic coatings promote the formation of a continuous water film on the substrate surface through high-density polar groups, thereby maintaining high transmittance. This strategy not only enables efficient anti-fogging under low-humidity conditions but also offers advantages such as simple processing and ease of scale-up.[11–13]

In recent years, numerous hydrophilic anti-fogging coatings have been successfully developed based on various materials and strategies. By constructing a poly(vinylsulfonic acid)-terminated surface on polyelectrolyte layers, a direc-

tional arrangement of hydrogen bonding networks can be achieved, enabling self-cleaning functionality on superhydrophilic surfaces.[14,15] To enhance the mechanical stability of hydrophilic coatings, hybrid films were prepared by crosslinking carboxyl-containing polyimide with poly(vinyl alcohol) through esterification/etherification reactions. The optimized crosslinked structure not only provides high water resistance and adhesion but also imparts impact resistance and abrasion durability.[16,17] To further adapt to dynamic environments such as temperature cycling, a host-guest supramolecular (HGSM) crosslinking strategy was proposed. By synergistically combining noncovalent interactions between β-cyclodextrin and adamantane with a covalent network, the coating can achieve rapid self-healing of cracks within 15 s.[18] This amphiphilic strategy, constructed *via* nanoscale hydrophilic-hydrophobic microdomain compartmentalization, exhibits unique advantages.[19–21] Nevertheless, significant limitations remain: these approaches often rely on multi-step reactions (*e.g.*, layer-by-layer assembly or photopolymerized template synthesis), resulting in complex processes and high costs. Most material designs focus solely on extending service lifetime by enhancing the adhesion of the polymer resin, while overlooking the potential of incorporating inorganic components to improve coating cohesion and abrasion resistance. Moreover, few studies have addressed the enhancement of UV-aging resistance through organic-inorganic hybridization.

The incorporation of inorganic components such as ZnO, TiO_2, CWO, or SiO_2 into polymer resin to prepare organic-inorganic hybrid anti-fogging coatings has been proposed.[22–24] These coatings combine the flexibility of organic materials with the stability of inorganic constituents. However, the absence of hydrogen bonding sites, large particle sizes, and poor dispersibility of the inorganic components hinder molecular-level organic-inorganic hybridization, limiting significant improvements in coating abrasion resistance and weatherability. In contrast, polyoxometalates (POMs), possessing abundant surface proton sites and oxygen-rich coordination structures, exhibit unique advantages in interface engineering within polymer composite systems.[25,26] The nanoscale, monodisperse nature of POMs in aqueous systems not only allows modulation of polymer crosslinking density to reduce residual stress but also enhances interfacial adhesion through strong proton-dipole interactions.[27–29] Moreover, the intramolecular charge-transfer transitions of POMs enable efficient ultraviolet (UV) absorption, mitigating UV-induced aging of the polymer resin under sunlight. POMs with unique structures can serve as inorganic functional components and be incorporated at the molecular level into highly adhesive polymer resin. This provides a viable strategy for developing durable, long-lasting anti-fogging hybrid coatings.

In this study, an amphiphilic organic-inorganic hybrid anti-fogging coating was designed based on an aqueous acrylic emulsion and POMs to create hydrophilic and hydrophobic domains. Specifically, a hydrophilic resin rich in ionic groups and hydroxyl functionalities was synthesized *via* emulsion polymerization and subsequently combined with POMs to prepare an aqueous superhydrophilic anti-fogging coating. By adjusting the ratio of hydrophilic to hydrophobic monomers, the coating achieves effective anti-fogging performance while suppressing excessive water adsorption during fogging, which could otherwise cause film swelling and wrinkling. The ratio of POMs to the polymer resin was optimized to tune the coating's cohesion, adhesion, and light transmittance. This enabled high abrasion resistance and weatherability on various substrates, including glass, agricultural films, and optical devices. Importantly, this simple method produces an aqueous superhydrophilic anti-fogging coating that is environmentally friendly and easily scalable. It shows significant potential for commercial applications.

EXPERIMENTAL

Materials

Sodium styrene sulfonate (SSNa) (≥90%, Aladdin), 2-hydroxyethyl methacrylate (98%, HEMA, Macklin, inhibitor removed by basic alumina), ethyl acrylate (99%, EA, Macklin, inhibitor removed by basic alumina), methyl methacrylate (99.5%, MMA, Macklin, inhibitor removed by basic alumina), sodium oleate (≥ 97%, NaOI, Aladdin), potassium persulfate (99.9%, KPS, Macklin), OP-10 (Macklin), sodium dodecyl sulfate (99%, SDS, Macklin), hydrated silicotungstic acid (97%, Aladdin), and basic alumina (100-200 mesh, Guoyao Reagents) were used as received unless otherwise specified.

Synthesis of the Acrylic Emulsion and Coating Solutions

To achieve a polymer resin with balanced adhesion, hydrophilicity, and mechanical stability, the acrylic emulsion was designed through the copolymerization of five functional monomers. The SSNa provides strongly hydrophilic sulfonate groups for rapid water absorption and anti-fogging. The HEMA offers hydroxyl groups that enhance both the coating's hydrophilicity and its adhesion to substrates *via* hydrogen bonding. EA and MMA serve as hydrophobic monomers to regulate the glass transition temperature and flexibility of the resin. Their hydrophobic nature also counterbalances the excessive water absorption tendency of the hydrophilic monomers, preventing film swelling. Notably, NaOI not only acted as a functional monomer but also served as a reactive surfactant, which could potentially participate in the copolymerization, further enhancing the anti-fogging durability of the resulting coating.

Acrylic emulsions were prepared *via* emulsion polymerization. OP-10 (0.1 g), potassium persulfate (KPS, 0.1 g), sodium dodecyl sulfate (SDS, 0.1 g), sodium styrene sulfonate (1.5 g), and sodium oleate (0.5 g) were dissolved in 40 g of deionized water and stirred at 1500 r/min for 30 min. Subsequently, 2.0 g of HEMA, 2.0 g of MMA, and 3.5 g of EA were added. The mixture was polymerized at 85 °C for 3 h. By adjusting the sodium styrene sulfonate to EA ratio (Table S1 in the electronic supplementary information, ESI), five emulsions (PAE-1 to PAE-5) were obtained. For coating solutions, 5 g of each acrylic emulsion was mixed with POMs at different mass ratios (Table S2 in ESI) and stirred at 80 °C for 2 h.

Coating Fabrication

5 g of each mixture was diluted with 50 g of deionized water to obtain the final coating solutions, denoted as PPOM-1, PPOM-2,

PPOM-3, PPOM-4, and PPOM-5. Glass substrates were sequentially ultrasonicated in deionized water and ethanol for 1 h each, repeated three times, and dried at 70 °C. The substrates were then subjected to argon plasma treatment (150 W, 5 min) before coatings were applied by dip-coating and cured at 60 °C for 2 h, as shown in Fig. 1.

Characterization

Fourier transform infrared spectroscopy (FTIR) spectra were recorded using a VERTEX 70 spectrometer. The acrylic emulsion was analyzed by ^{1}H-NMR spectroscopy (AVANCE III HD 600 MHz) using DMSO-d_6 as solvent to determine the proton peak positions. Differential scanning calorimetry (DSC, TA DSC25) was used to determine glass transition temperatures. Visible-light transmittance spectra were measured with a UV-3600 Plus spectrophotometer. The morphology and energy dispersive system (EDS) element mappings were characterized using a scanning electron microscope (SEM, Gemini300). Static water contact angle (WCA) was measured using a JC2000D2G goniometer. Adhesion was evaluated by the cross-cut method and observed under a fluorescence microscope (Leica DM2500). Abrasion resistance was tested using a wear tester, and UV-aging performance was assessed in a Q-LAB/SPPAY chamber. The surface roughness was investigated using a Bruker Dimension Icon SPM atomic force microscope (AFM). The visible-light transmittance (T_{vis}, 380–780 nm) of the coating was calculated as described in Eq. (1)

$$T_{vis} = \frac{\int \varphi_{vis}(\lambda)T(\lambda)d\lambda}{\int \varphi_{vis}(\lambda)d\lambda} \quad (1)$$

where $T(\lambda)$ represents the transmittance at wavelength λ, $\varphi_{vis}(\lambda)$ represents the light sensitivity of human eyes, and $\varphi_{NIR}(\lambda)$ represents the solar irradiation intensity (AM 1.5).

RESULTS AND DISCUSSION

Structural Characterization of the Coatings

In this copolymer system, MMA and EA are used to balance coating flexibility, while HEMA enhances adhesion and hydrophilicity through its hydroxyl groups. The SSNa monomer acts as a reactive surfactant, stabilizing the emulsion and improving wettability. By adjusting the SSNa/EA ratio, a balance between the fog resistance and water resistance of the coating can be achieved. To investigate the changes in polymer sequence structure with varying monomer feed ratios, ^{1}H-NMR spectra of different PAE resins were conducted in DMSO-d_6 (Fig. S1 in ESI). The spectra revealed a characteristic peak at 7.34 ppm, corresponding to the aromatic protons of SSNa. Its integrated area showed a strong positive correlation with the monomer feed ratio. This confirmed that this hydrophilic monomer can be quantitatively incorporated into the polymer chain. The broad peak at 4.77 ppm was unequivocally assigned to the hydroxyl proton resonance of HEMA. The peak at 4.04 ppm, attributed to the ethoxy methylene group (—O—CH_2—) of EA, decreased in intensity with a reduction in the EA feed ratio. This directly reflected the controllable regulation of copolymer composition. These spectral analyses confirm the presence of the characteristic functional groups of each monomer and their concentration-dependent variations. However, further quantitative analysis of the proportions of structural units in the polymer is hindered by residual signals from the emulsifier and initiator. Notably, the monomer conversion rate was determined to be approximately 99.8% by gravimetric analysis. Therefore, the actual monomer ratio in the polymer backbone can be considered nearly identical to the feed ratio.

FTIR spectra were used to analyze the molecular structure of the hydrophilic resin and its hybridization with POMs. As shown in Fig. 2(a), the pure polymer shows characteristic bands at 1288 cm^{-1} (S=O stretching), 1546 cm^{-1} (aromatic vi-

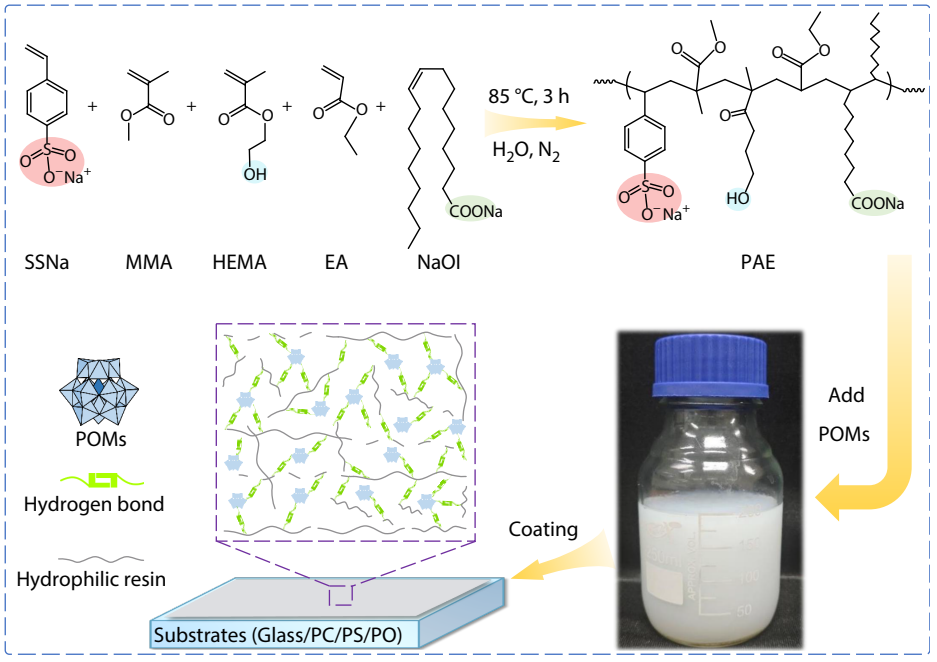

Fig. 1 Schematic illustration of PPOM coating preparation.

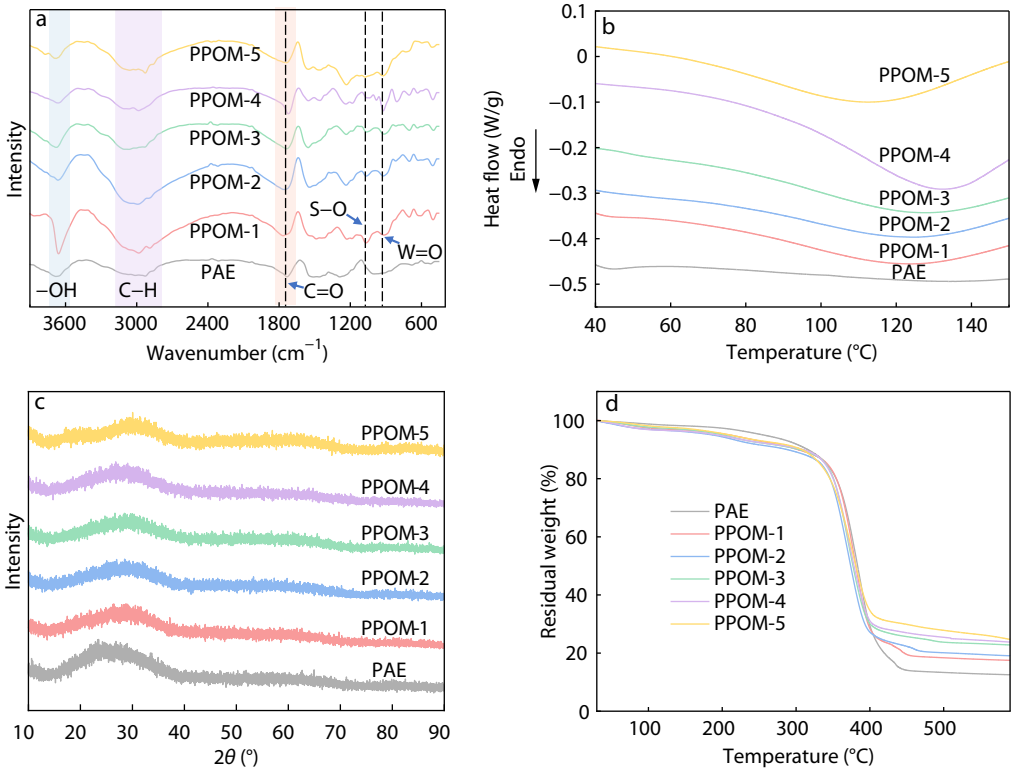

Fig. 2 Characterizations of PAE and PPOMs with different POMs loadings: (a) FTIR spectra; (b) DSC curves; (c) XRD patterns; (d) TGA curves.

bration), and 1733 cm^{-1} (C=O stretching),[30,31] attributed to sodium p-styrenesulfonate and hydroxyethyl methacrylate units. These results confirm the successful synthesis of the designed resin. After incorporating POMs, new bands at 1180 cm^{-1} (Si—O asymmetric stretching), 979 cm^{-1} (W=O stretching), and 921 cm^{-1} (W—O—W stretching) appear,[32,33] indicating the homogeneous hybridization between POMs and resin. Notably, the enlarged illustration shown in Fig. S2 (in ESI) clearly shows that the —OH band has shifted from 3682 cm^{-1} to 3660 cm^{-1}, and the C=O peak has shifted from 1733 cm^{-1} to 1720 cm^{-1}, both exhibiting a significant redshift. These shifts are attributed to multilevel hydrogen bonding interactions between the bridging oxygen of POMs (W—O—W) and the sulfonic acid (—SO_3H), hydroxyl (—OH), and ester (—COOR) groups in the copolymer. This strong molecular interaction confirms the formation of a hydrogen-bonded network, which provides the basis for enhanced cohesion and contributes to the coating's abrasion resistance.

To further elucidate the interactions between POMs and the polymer units, DSC analyses were performed on the solid PPOM components, as shown in Fig. 2(b). The pristine acrylic resin exhibits a glass transition temperature (T_g) of 88.3 °C. In contrast, the T_g of PPOM-4 coatings increases progressively with the POMs content, reaching a maximum of 101.5 °C. This pronounced T_g elevation can be attributed to two synergistic effects: (1) hydrogen bonding between POMs and copolymer chains restricts segmental mobility and reduces the free volume; (2) the rigid inorganic nano-units of POMs act as physical crosslinking sites, suppressing the rotational relaxation of the polymer backbone.[34] Moreover, the broadened glass transition region observed for PPOMs suggests the presence of dynamic hydrogen bond dissociation-reformation processes within the hybrid network. However, once the POMs content reaches 2.9 wt%, the T_g of PPOM-5 declines to 83.1 °C as excessive POMs induce phase separation and loose polymer regions near aggregates.[35] These results highlight the significant regulatory role of POMs in tailoring the thermodynamic behavior of the coating and further confirm the effective hybridization between the organic and inorganic components.

To further investigate the influence of the introduction and content of POMs on the movement of hydrophilic resin chain segments, XRD and TGA analysis were conducted on the solid components of the PPOMs (Figs. 2c and 2d). Both the pure PAE and the PPOMs with different POMs loadings exhibit broad amorphous diffraction. The results indicate that POMs do not induce crystallization, which is essential for maintaining high transparency. A noticeable shift of the diffraction peak toward higher angles is observed. According to Bragg's law, this peak shift reflects a reduced interchain spacing, suggesting stronger intermolecular interactions.[36] Such homogeneous dispersion of POMs within the amorphous polymer resin, facilitated by multiple hydrogen bonding interactions, forms a hybridized crosslinking network. This structure enables dynamic hydrogen bond dissipation for toughness enhancement while avoiding light-scattering losses that would arise from filler aggregation. No distinct diffraction peaks corresponding to POMs are detected, likely due to its low loading. Collectively, these characterizations confirm successful organic-inorganic hybridization, providing a structural basis for the observed improvements in coating performance.

Anti-fogging Properties of the Coatings

To investigate the influence of polymer chain composition on

anti-fogging performance, coatings with varying monomer ratios (Table S1 in ESI) were evaluated by placing each sample 2 cm above 80 °C hot water for 1 min (Fig. S3 in ESI). The PAE-1 coating exhibited distinct fog formation, attributed to its low fraction of highly hydrophilic sodium p-styrenesulfonate. The dominance of EA and MMA hydrophobic segments hindered the coating's ability to rapidly absorb vapor and form a continuous water film. As the proportion of sodium p-styrenesulfonate increased, the anti-fogging performance improved. When its content reached 10%, and the hydrophobic monomers were reduced to below 40%, the coatings maintained high transparency in 80 °C hot water. The underlying patterns remained clearly visible, indicating that all four coatings exhibited reliable anti-fogging behavior. However, when the sodium p-styrenesulfonate content exceeded 20% (PAE-4, PAE-5), excessive sulfonic groups continuously absorbed water during prolonged anti-fogging operation (5 min), causing swelling and stress accumulation. The water film on the coating surface became too thick, leading to refraction and scattering of visible light.[19] The underlying pattern was still visible, but the image edges showed noticeable distortion (Fig. S4 in ESI). Additionally, the reduction in HEMA monomers would weaken the interaction between the coating and the substrate as the number of hydroxyl groups decreased. In contrast, coatings with slightly lower sodium p-styrenesulfonate content (PAE-2 and PAE-3) maintained clear and intact images even after prolonged exposure to abundant water vapor. This is mainly attributed to the higher content of hydrophobic ethyl acrylate, which prevented excessive thickening of the water film.

Therefore, rapid water film formation can be achieved while limiting film thickness by balancing hydrophilic and hydrophobic components, enabling long-lasting anti-fogging performance. To further determine the optimal sodium p-styrenesulfonate content, abrasion tests were conducted on PAE-2 and PAE-3 under a 500 g load. The results show that PAE-2 exhibited a significant loss of anti-fogging performance after 250 abrasion cycles. In contrast, PAE-3 maintained excellent anti-fogging behavior after 550 cycles, likely due to the stronger polarity of sodium p-styrenesulfonate compared with hydrophobic ethyl acrylate (Fig. S5 in ESI). The higher content of sodium p-styrenesulfonate in PAE-3 enhances interfacial interactions with the substrate, improving abrasion resistance.

To investigate the effect of POMs on coating performance, the visible-light transmittance (400–800 nm) and anti-fogging tests were conducted on a series of PPOM coatings with varying POMs content. As shown in Fig. 3(a), PPOM-1, PPOM-2, PPOM-3, and PPOM-4 coatings all exhibited a transmittance of >88%. However, the transmittance of PPOM-5 coating decreased slightly to 84% when the POMs content increased to 2.9 wt%. This reduction was likely due to light scattering arising from the refractive-index mismatch between POMs and the acrylic polymer resin. Subsequently, all coatings exhibited ultra-low WCA and excellent anti-fogging performance, as shown in Fig. 3(d). This performance is mainly attributed to the strong hydrophilic ionic groups of sodium p-styrenesulfonate and the abundant hydroxyl groups on the POMs surface, which rapidly absorb water vapor and form a

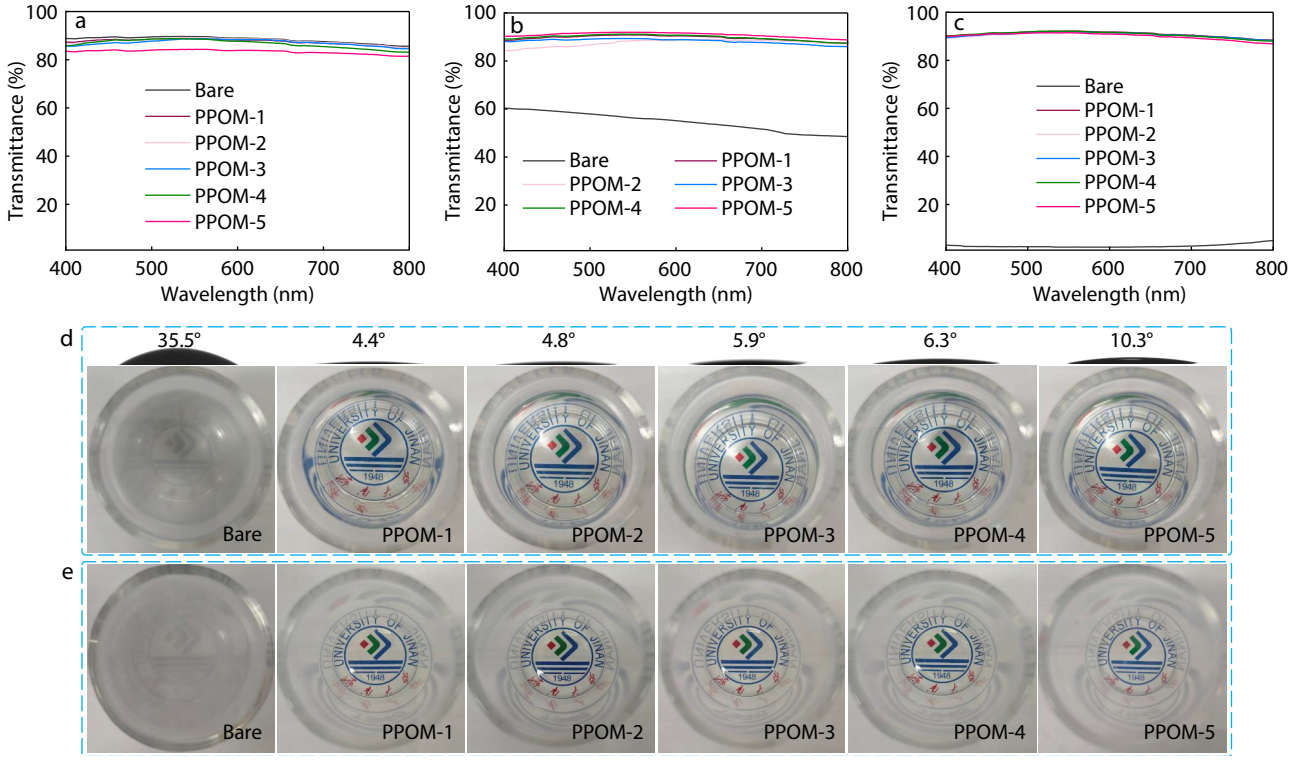

Fig. 3 (a) Visible-light transmittance of bare glass and PPOM coatings; (b) Visible-light transmittance of bare glass and PPOM coatings after anti-fogging test; (c) Visible-light transmittance of bare glass and PPOM coatings after anti-frosting test; (d) WCA and photographs of bare glass and PPOM coatings under 80 °C hot water; (e) Anti-frosting photographs of bare glass and PPOM coatings at −15 °C.

https://doi.org/10.1007/s10118-026-3690-x

uniform water film on the glass surface. In addition, the transmittance of bare glass and the PPOM coatings was evaluated over hot water at 80°C (Fig. 3b). The transmittance of bare glass dropped to 60%, whereas that of the PPOM coatings slightly increased (about 90%), further demonstrating the excellent anti-fogging and anti-reflective property of the PPOM coatings. However, the coating lost its anti-fogging capability when the POMs content increased to 3.2 wt% (Fig. S6 in ESI). Excessive POMs formed a dense hydrogen bond network with polymer chains, reducing the free volume in the polymer network. As a result, water vapor could not diffuse into the limited polymer chain pores, leading to visible fog formation on the coating surface.[23] Satisfyingly, the kilogram-scale PPOM coating dispersion exhibits excellent adhesion and anti-fogging performance on various substrates, including polyolefin (PO), polystyrene (PS), and polycarbonate (PC) (Figs. S7 and S8 in ESI).

To evaluate the anti-fogging performance of the coatings under more severe conditions, an anti-frosting test was conducted. Samples were stored at −15 °C for 30 min and then transferred to room temperature to observe frost formation. As shown in Fig. 3(e), bare glass quickly developed visible frost, causing the transmittance to drop sharply to 3% (Fig. 3c). In contrast, glass coated with PPOMs maintained high transparency. The transmittance was even 1%–2% higher than that of unfrosted bare glass, likely because the water film formed on the surface reduced the refractive index difference between air and glass, providing a slight anti-reflective effect. The frost-free behavior of PPOM coatings is likely due to the presence of non-freezing bound water within the POMs, which prevents ice formation.[37] These results demonstrate that PPOM coatings exhibit excellent anti-fogging and anti-frosting performance, indicating broad potential application prospects.

Durability Performance of the Coatings

In addition to the anti-fogging performance, the adhesion between the coating and the substrate plays a critical role in determining the long-term durability of the system. Conventional hydrophilic coatings often suffer from interfacial failure due to weak bonding with the substrate, leading to wrinkling and exfoliation. To evaluate the adhesion between PPOM coatings and substrate, cross-cut adhesion tests were conducted for coatings with different POMs contents, as shown in Fig. S9 (in ESI). A series of parallel cuts with 1 mm spacing was made on the coating surface using a multi-blade cutter to form a regular grid. Subsequently, a 3M adhesive tape was then pressed onto the grid under a uniform load of 500 g and rapidly peeled off. The results show that the peeling area of PPOM-1 and PPOM-2 accounted for approximately 5-10% of the total grid area, while PPOM-3 exhibited less than 5% peeling. PPOM-4 and PPOM-5 showed no noticeable detachment, indicating superlative adhesion. Clearly, the adhesion strength of the coating increases with increasing POMs content. The abundant protons and oxygen-rich surface of POMs, combined with the abundant hydroxyl groups derived from HEMA in the polymer resin, collectively form a robust interfacial network with the plasma-treated substrate, thereby significantly improving the overall bonding strength.

Mechanical abrasion after surface contamination is one of the main causes of anti-fogging failure, making coating abrasion resistance critical for service life. To evaluate the effect of POMs incorporation on abrasion resistance, abrasion tests under a 500 g load were performed on PAE-3 and PPOM-4 coatings, and PPOM-4 was selected for comparison with PAE (Fig. 4a). The WCA of PAE-3 increased to 14.98° after 600 cycles, and most areas lost anti-fogging performance in the 80 °C hot-fog test. Furthermore, the WCA of PAE-3 increased to 30.06° after 1200 cycles. In contrast, PPOM-4 maintained a WCA increase from 6.7° to only 12.9° after 1200 cycles, with no significant change in anti-fogging performance (Fig. 4b). These results demonstrate that POMs incorporation markedly improves the abrasion resistance of the coatings. Additionally, compared with anti-fogging coatings reported in the literature, the PPOM-4 coating exhibits superior abrasion resistance (Table S3 in ESI).

To investigate the origin of improved abrasion resistance, SEM characterization was performed on PAE and PPOM coatings (Fig. 4c). The pure polymer coating exhibits a distinctly granular surface. After incorporating POMs, the PPOM organic-inorganic hybrid coating exhibits a dense and smooth morphology. FTIR analysis confirmed hydrogen bonding between POMs and the polymer resin. It is inferred that POMs form a multi-level hydrogen bond network with sulfonic acid and hydroxyl groups in the polymer chains *via* a bridging oxygen structure. This network effectively enhances the interfacial interaction between POMs and acrylic polymer chains, optimizing the coating's surface microstructure.[38] This improvement is attributed to the formation of multiple hydrogen bonding interactions between POMs and the polymer chains, as confirmed by FTIR analysis. It is inferred that POMs form a multi-level hydrogen bond network with sulfonic acid and hydroxyl groups in the polymer chains *via* their bridging oxygen structure. This network effectively fills micro-voids between acrylic segments, thereby optimizing the coating's surface microstructure.

To further assess the surface characteristics of the coatings, AFM was employed to measure the roughness of PPOM and PAE coatings (Fig. 4d). The average roughness (R_q) decreased from 5.60 nm for the PAE coating to 4.09 nm for the PPOM coating. The surface morphology and roughness of PPOM-4 (Fig. S10 in ESI) coating were examined after 1200 abrasion cycles, with the roughness of the coating being quantified as 5.38 nm, indicating a minimal increment of 1.29 nm. This surface smoothening can significantly reduce the friction coefficient and alleviate interfacial stress concentration, thereby prolonging coating lifetime. In addition, SEM-EDS mapping (Fig. 4e) shows that C, O, S, W, and Si are homogeneously distributed across the coating surface. The characteristic elements of POMs (W and Si) do not show aggregation, indicating excellent compatibility between POMs and the acrylic emulsion with no phase separation. Cross-sectional SEM analysis of the coating (Fig. S10 in ESI) revealed a uniform thickness of 1.615 μm. Elemental mapping confirmed a homogeneous distribution of POMs throughout the coating, with no evidence of surface agglomeration. The absence of phase separation prevents light scattering, providing the basis for simultaneously achieving high transparency and durability. The uniform hybrid structure enhances cohesion and mechanical stability through hydrogen bond crosslinking. In ad-

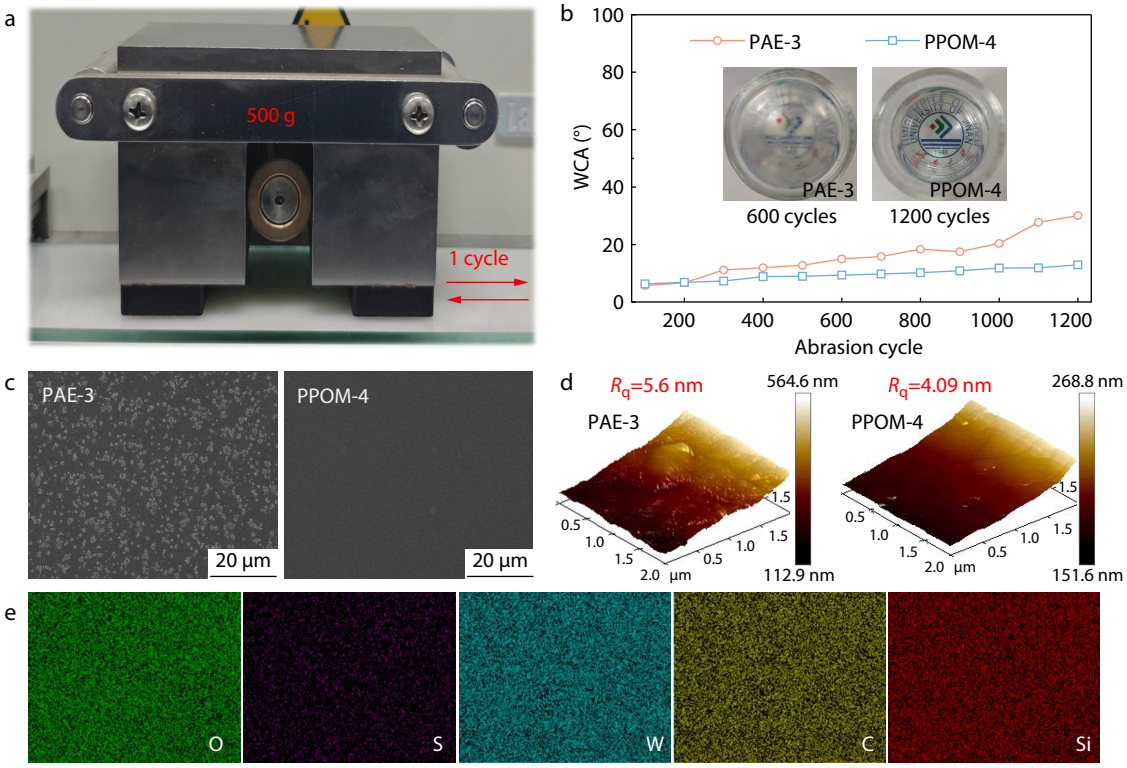

Fig. 4 (a) Photograph of the abrasion test; (b) WCA of PPOM-4 and PAE-3 coatings after different abrasion cycles; (c) SEM micrographs of the PAE-3 and PPOM-4 coating surfaces; (d) AFM images of PAE-3 and PPOM-4 coatings; (e) SEM element mappings of PPOM-4 coating.

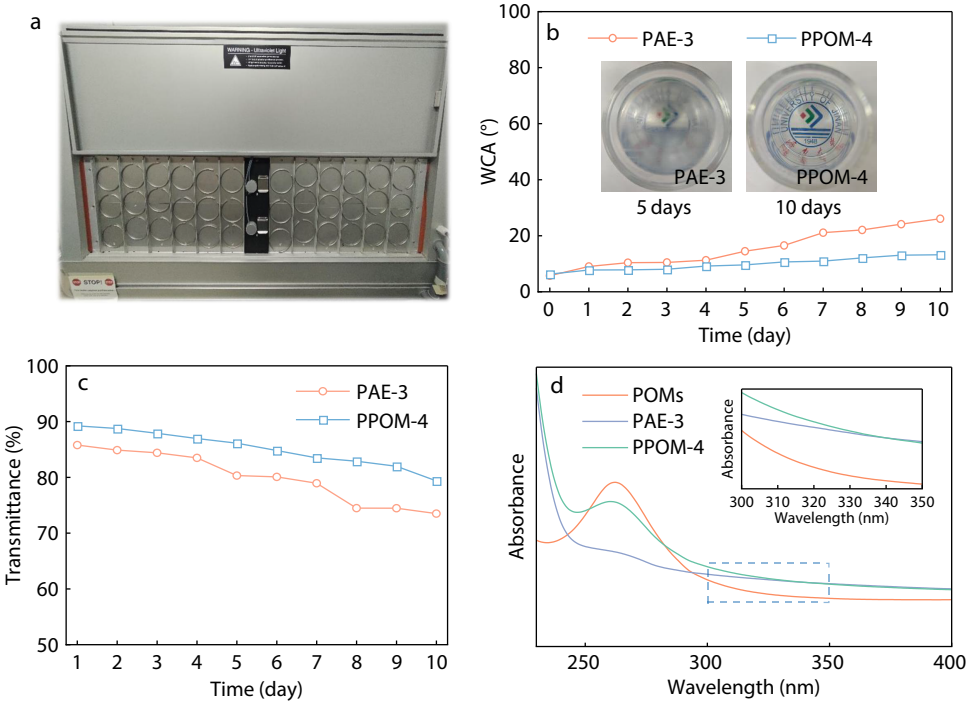

Fig. 5 (a) Photograph of the UV-aging test; (b) WCA of PPOM-4 and PAE-3 coatings after different UV-aging durations; (c) Visible-light transmittance of PPOM-4 and PAE-3 coatings under different UV-aging durations; (d) UV absorption spectra of POMs, PAE-3, and PPOM-4.

dition, the oxygen-rich surface of POMs can form bonds with the corona-treated glass substrate, which further improves adhesion and abrasion resistance.

Prolonged exposure of anti-fogging coatings to complex environments, including ultraviolet (UV) radiation, can cause bond scission or molecular rearrangement within the poly-

https://doi.org/10.1007/s10118-026-3690-x

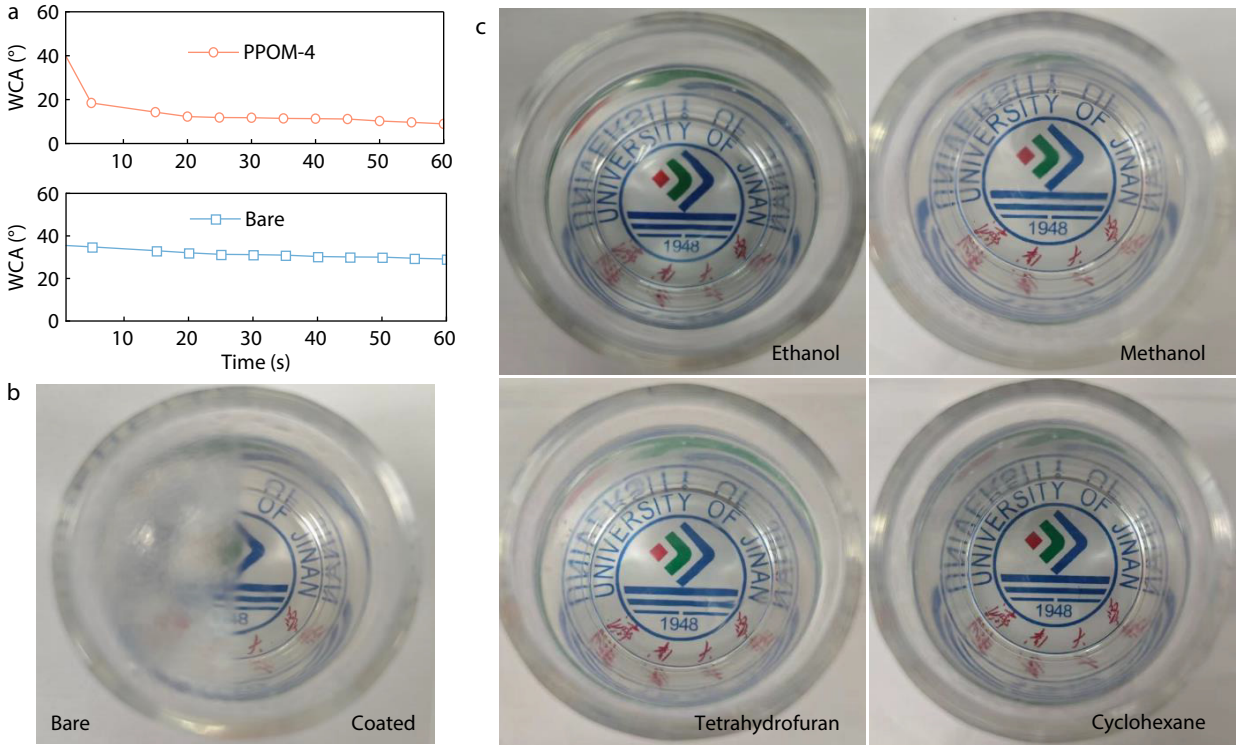

Fig. 6 (a) Time-dependent WCAs of PPOM coatings and bare glass after 48 h of immersion at 25 °C; (b) Anti-fogging behavior following 48 h water immersion; (c) Anti-fogging behavior after 240 h immersion in ethanol, methanol, tetrahydrofuran, and cyclohexane.

mer resin, which may lead to interfacial delamination from the substrate. Such aging processes can eventually cause the loss of anti-fogging functionality or a decline in optical transmittance. Therefore, UV-accelerated aging tests were conducted to evaluate the stability and structural durability of the coatings, ensuring the long-term anti-fogging performance under realistic service conditions. The variation in WCA for the PAE coating and PPOM coatings was monitored under conditions of 60 °C and an irradiance of 0.68 W/m^2, as shown in Fig. 5(a). The pure polymer coating exhibited a rapid loss of anti-fogging behavior after 5 days of UV exposure, with its contact angle increasing to 16.5° due to extensive UV-induced degradation of the polymer chains. In contrast, although the contact angle of the PPOM coatings slightly increased to 13.2° after 10 days of exposure, desirable anti-fogging performance was still maintained (Fig. 5b). By comparing the visible-light transmittance of the PAE-3 and PPOM-4 coatings after different durations of UV-accelerated aging, it can be seen that the PPOM coating exhibits a superior anti-reflective effect compared with PAE-3. The results suggest that the incorporation of POMs effectively enhances the weathering resistance of the coating (Fig. 5c). The enhanced UV-aging resistance mainly stems from the abundant Si—O and W—O bonds in the POMs structure.[39] These bonds effectively absorb UV light (Fig. 5d), which reduces UV damage to the polymer resin and improves the overall stability of the coating.[40,41]

Moreover, the hydrophilic components in conventional anti-fogging coatings tend to dissolve in various solvents, leading to the loss of anti-fogging performance. To assess solvent resistance, the PPOM coatings were tested in both water and organic solvents. As shown in Fig. 6(a), the contact angle remained at about 10° even after 48 h of immersion in distilled water at 25 °C, indicating that the coating retained high hydrophilicity and stable anti-fogging performance (Fig. 6b). In addition, the PPOM coatings exhibited excellent resistance to organic solvents. After 240 h of immersion in both polar and nonpolar solvents, the coatings still maintained outstanding anti-fogging properties (Fig. 6c). This robustness can be attributed to the abundant proton sites and oxygen-rich coordination structure on the POMs surface, which enables strong bonding with the substrate. Along with interfacial hydrogen bonding between POMs and the acrylic polymer chains, a dense and stable network is formed, making it difficult for solvents to penetrate and thus ensuring superior solvent resistance.

CONCLUSIONS

In this work, an organic-inorganic anti-fogging coating was developed by integrating POMs with a designed aqueous polymer resin. POMs provide abundant proton sites and oxygen-rich coordination. Optimizing the ratio of hydrophilic to hydrophobic monomers and POMs content yielded coatings with excellent anti-fogging/anti-frosting performance, addressing the poor abrasion resistance and limited environmental durability in conventional coatings. Strong interfacial interactions among coatings with various substrates, including glass, PS, PO films, and PC, resulted in desirable adhesion. Importantly, the incorporation of POMs significantly reduced the surface roughness of the coating and enhanced cohesion based on multiple hydrogen bonding interactions between POMs and the polymer resin,

resulting in excellent abrasion resistance. The coatings maintained anti-fogging performance after 1200 abrasion cycles under 500 g. Accelerated UV aging at 0.68 W/m^2 and 60 °C for 240 h showed that POMs incorporation effectively protects the polymer resin from photodegradation under sunlight. The organic solvent-free synthesis and facile scalability indicate broad practical and commercial potential for this coating.

Conflict of Interests

The authors declare no interest conflict.

Electronic Supplementary Information

Electronic supplementary information (ESI) is available free of charge in the online version of this article at http://doi.org/10.1007/s10118-026-3690-x.

Data Availability Statement

The data supporting the findings of this study are available from the corresponding author upon reasonable request.

ACKNOWLEDGMENTS

This work was financially supported by Shandong Province Postdoctoral Innovation Project (No. SDCX-ZG-202302017), and Natural Science Foundation of Shandong Province (Nos. ZR2022QB045 and ZR2025QC564).

REFERENCES

1 Gao, H. P.; Xing, Z. T.; Chang, S. Y.; Zhao, F. Y.; Zhang, H. L.; Meng, Z.; Han, Z. W.; Liu, Y. Bioinspired multifunctional antifogging surfaces: progress, AI design and challenges. *Prog. Mater. Sci.* **2026**, *155*, 101530.

Graphical Abstract

Durable Anti-fogging and Abrasion-resistant Coatings Based on Polyoxometalates-Hydrophilic Resin Composites with Enhanced Cohesion and Adhesion

Xu Yang, Shu-Di Ying, Cong-Cong Zhai, Yu-Lin Yin, Jian-chao Hou, Pan-Pan Zhao, Wen-Ting Li, Shuai-Jun Yang, Jia-Chen Ma, and Xu-Chuan Jiang

University of Jinan; Huzhou College; Shandong Institute of Non-Metallic Materials

An organic-inorganic hybrid anti-fogging coating composed of polyoxometalates and hydrophilic resin, with enhanced adhesion and cohesion, achieves high abrasion resistance, UV stability, and durable superhydrophilicity for various substrates.

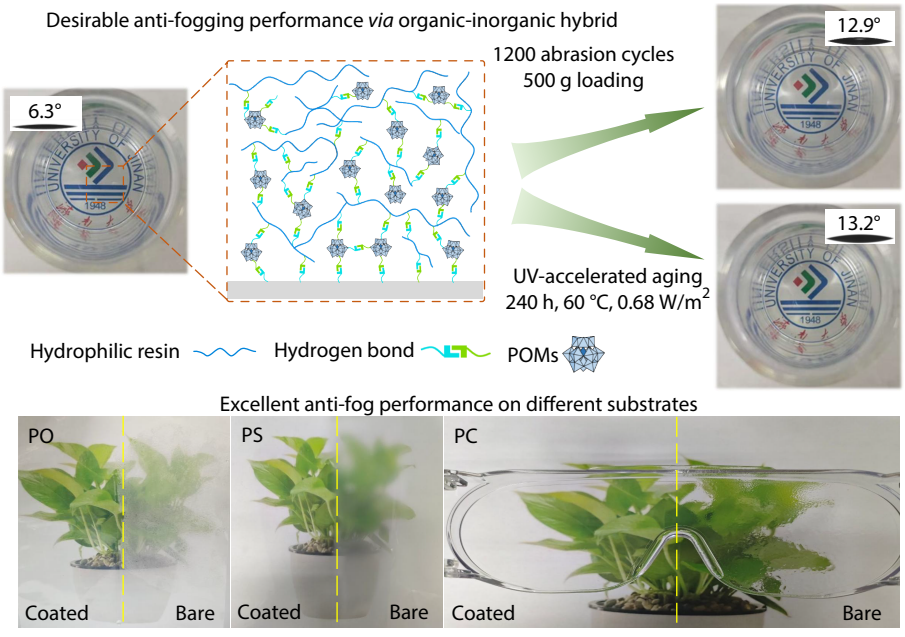

2 Gong, X. D.; Yu, H. J.; Wang, L.; Liu, X. W.; Ren, S. N.; Huang, Y. D.; Huang, Z. K. Recent progress in the mechanisms, preparations and applications of polymeric antifogging coatings. *Adv. Colloid. Interface Sci.* **2022**, *309*, 102794.
3 Haechler, I.; Ferru, N.; Schnoering, G.; Mitridis, E.; Schutzius, T. M.; Poulikakos, D. Transparent sunlight-activated antifogging metamaterials. *Nat. Nanotechnol.* **2023**, *18*, 137−144.
4 Han, Z. W.; Feng, X. M.; Guo, Z. G.; Niu, S. C.; Ren, L. Q. Flourishing bioinspired antifogging materials with superwettability: progresses and challenges. *Adv. Mater.* **2018**, *30*, 1704652.
5 Li, Z. Y.; Liu, Y. Z.; Liu, Y. B.; Feng, K.; Li, J.; Wu, Y.; Zhou, F. Robust transparent photothermal omniphobic coating for efficient anti/deicing and antifogging. *ACS Appl. Mater. Interfaces* **2024**, *16*, 35805−35814.
6 Walker, C.; Mitridis, E.; Kreiner, T.; Eghlidi, H.; Schutzius, T. M.; Poulikakos, D. Transparent metasurfaces counteracting fogging by harnessing sunlight. *Nano Lett.* **2019**, *19*, 1595−1604.
7 Wang, D. H.; Sun, Q. Q.; Hokkanen, M. J.; Zhang, C. L.; Lin, F. Y.; Liu, Q.; Zhu, S. P.; Zhou, T. F.; Chang, Q.; He, B.; Zhou, Q.; Chen, L. Q.; Wang, Z. K.; Ras, R. H. A.; Deng, X. Design of robust superhydrophobic surfaces. *Nature* **2020**, *582*, 55−59.
8 Yoon, J. S.; Ryu, M.; Kim, H.; Ahn, G. N.; Yim, S. J.; Kim, D. P.; Lee, H. Wet-style superhydrophobic antifogging coatings for optical sensors. *Adv. Mater.* **2020**, *32*, 2002710.
9 Kim, H.; Lee, Y.; Jung, S.; Lee, H. Micropatterned hydrogel-elastomer hybrids for flexible wet-style superhydrophobic antifogging tapes. *Adv. Funct. Mater.* **2024**, *34*, 2401869.
10 Zhang, Y.; Liu, Q. L.; Li, J.; Yao, H. C.; Hou, Y. H.; Hou, J. Z. Large-scale fabrication of flexible antiglare film with superhydrophobic surface: Toward high transmittance and high haze. *Chem. Eng. J.* **2025**, *511*, 161805.
11 Hovish, M. Q.; Hilt, F.; Rolston, N.; Xiao, Q. R.; Dauskardt, R. H. Open air plasma deposition of superhydrophilic titania coatings. *Adv. Funct. Mater.* **2019**, *29*, 1806421.
12 Jin, T. H.; Peydayesh, M.; Li, M. Q.; Yao, Y.; Wu, D.; Mezzenga, R. Functional coating from amyloid superwetting films. *Adv. Mater.* **2022**, *34*, 2205072.
13 Li, N.; Xu, Z.; Zheng, S.; Dai, H. Y.; Wang, L.; Tian, Y.; Dong, Z. C.; Jiang, L. Superamphiphilic TiO_2 composite surface for protein antifouling. *Adv. Mater.* **2021**, *33*, 2003559.
14 Wang, R.; Cheng, C. L.; Wang, H. Y.; Tao, Q.; Wang, D. Y. A simple poly(vinyl sulfonate) coating for all-purpose, self-cleaning applications: Molecular packing density-defined surface superhydrophilicity. *Adv. Funct. Mater.* **2023**, *33*, 2301085.
15 Wu, Y. L.; Dong, L.; Shu, X.; Yang, Y.; Feng, P.; Ran, Q. P. Recent advancements in photothermal anti-icing/deicing materials. *Chem. Eng. J.* **2023**, *469*, 143924.
16 Lee, J.; Kim, Y.; Kwak, G. High-durability anti-fog coating based on carboxyl-promoted anti-yellowing cross-linkable hybrid adhesive material of polyvinyl alcohol and polyimide. *Small* **2025**, *21*, 250307.
17 Altınışık, S.; Kortun, A.; Nazlı, A.; Cengiz, U.; Koyuncu, S. PEG-functionalized carbazole-based polymers for UV-protected hydrophilic glass coatings. *Prog. Org. Coat.* **2023**, *175*, 107352.
18 Lu, P. P.; Xu, J. Y.; Tian, W. J.; Zhang, C. C.; Niu, S. C.; Zhao, J.; Ming, W. H.; Ren, L. Q. Robust antifogging coatings with ultra-fast self-healing performances through host-guest strategy. *Chem. Eng. J.* **2023**, *465*, 142868.
19 Shi, J. H.; Xu, L. J.; Qiu, D. Effective antifogging coating from hydrophilic/hydrophobic polymer heteronetwork. *Adv. Sci.* **2022**, *9*, 2200072.
20 Mossayebi, Z.; Shabani, S.; Easton, C. D.; Gurr, P. A.; Simons, R.; Qiao, G. G. Amphiphilic nanoscale antifog coatings: Improved chemical robustness by continuous assembly of polymers. *Small* **2024**, *20*, 2402114
21 Liu, B. Y.; Zeng, J. S.; Li, P. F.; Kui, M. H.; Li, J. P.; Chen, K. F. Development of flexible nanocellulose-based composites with enhanced hydrophobicity and improved haze for efficient light management in solar cells. *Chem. Eng. J.* **2024**, *498*, 155273.
22 Zhang, C. J.; Liu, B. T.; Yu, S. Y.; Li, J. H.; Liu, Q.; Zhang, S. H.; Jian, X. G.; Weng, Z. H. Long-lasting and stable anti-fog coating combined with active and passive strategy. *Nat. Commun.* **2025**, *16*, 9003.
23 Yang, E. F.; Hao, D. Z.; Wang, P.; Luo, X. F.; Tian, Y.; Jiang, L. Facile formation of durable SiO_2-TiO_2 coatings on plastic films for self-cleaning and antifogging. *ACS Appl. Mater. Interfaces* **2025**, *17*, 3973−3981.
24 Jeon, Y.; Nagappan, S.; Li, X. H.; Lee, J. H.; Shi, L. Y.; Yuan, S.; Lee, W. K.; Ha, C. S. Highly transparent, robust hydrophobic, and amphiphilic organic-inorganic hybrid coatings for antifogging and antibacterial applications. *ACS Appl. Mater. Interfaces* **2021**, *13*, 6615−6630.
25 Xie, X. M.; Jiang, Y. L.; Yao, X. M.; Zhang, J. Q.; Zhang, Z. L.; Huang, T. P.; Li, R. H.; Chen, Y. F.; Li, S. L.; Lan, Y. Q. A solvent-free processed low-temperature tolerant adhesive. *Nat. Commun.* **2024**, *15*, 5017.
26 Anyushin, A. V.; Kondinski, A.; Parac-Vogt, T. N. Hybrid polyoxometalates as post-functionalization platforms: From fundamentals to emerging applications. *Chem. Soc. Rev.* **2020**, *49*, 382−432.
27 Yang, J. W.; Bai, R. B.; Chen, B. H.; Suo, Z. G. Hydrogel adhesion: A supramolecular synergy of chemistry, topology, and mechanics. *Adv. Funct. Mater.* **2019**, *30*, 1901693.
28 Cameron, J. M.; Guillemot, G.; Galambos, T.; Amin, S. S.; Hampson, E.; MallHaidaraly, K.; Newton, G. N.; Izzet, G. Supramolecular assemblies of organo-functionalised hybrid polyoxometalates: From functional building blocks to hierarchical nanomaterials. *Chem. Soc. Rev.* **2022**, *51*, 293−328.
29 Liu, J. C.; Zhao, J. W.; Streb, C.; Song, Y. F. Recent advances on high-nuclear polyoxometalate clusters, Coordin. *Chem. Rev.* **2022**, *471*, 214734.
30 Tumuluri, U.; Li, M. J.; Cook, B. G.; Sumpter, B.; Dai, S.; Wu, Z. L. Surface structure dependence of SO_2 interaction with ceria nanocrystals with well-defined surface facets. *Phys. Chem. C* **2015**, *119*, 28895−28905.
31 Garrido, M.; Naranjo, A.; Perez, E. M. Characterization of emerging 2D materials after chemical functionalization. *Chem. Sci.* **2024**, *15*, 3428−3445.
32 Liu, Y. F.; Bildan, D.; Zhuge, X. Q.; Liu, T.; Zhong, H. Y.; Luo, Z. H.; Lei, H. H.; Luo, K.; Ren, Y. R.; Bayati, M.; Liu, X. T. Composite gel polymer electrolyte for high-performance flexible zinc-air batteries. *Small* **2025**, *21*, 2408015.
33 Li, J. Y.; Xiong, J.; Huang, H. X.; Zhang, M.; Zhu, W. S.; Di, J. Significantly enhanced surface oxygen vacancies over $W_{18}O_{49}$ *via* Mo doping and plasma-induced surface reconstruction for oxidative desulfurization. *Sep. Purif. Technol.* **2023**, *318*, 123948.
34 Shen, J. X.; Lin, X. S.; Liu, J.; Li, X. Effects of Cross-link density and distribution on static and dynamic properties of chemically cross-linked polymers. *Macromolecules* **2018**, *52*, 121−134.
35 Hooper, J. B.; Schweizer, K. S. Theory of phase separation in polymer nanocomposites. *Macromolecules* **2006**, *39*, 5133−5142.
36 Ali, Y.; Sharma, K.; Kumar, V.; Sonkawade, R. G.; Dhaliwal, A. S. Polypyrrole microspheroidals decorated with Ag nanostructure: Synthesis and their characterization. *Appl. Surf. Sci.* **2013**, *280*, 950−956.
37 Zhang, D.; Chen, H.; Zhang, Y. X.; Yang, J. T.; Chen, Q.; Wu, J.; Liu, Y. L.; Zhao, C.; Tang, Y. J.; Zheng, J. Antifreezing hydrogels: From mechanisms and strategies to applications. *Chem. Soc. Rev.* **2025**, *54*, 5292−5341.
38 Yang, C. G.; Chen, C.; Tao, D. C.; Yan, K.; You, H. N.; Liu, Q. Z.; Wang,

W. W.; Wang, D. Facile design of nanofiber composite film with multi-level crosslinked enhanced structure using carbon nanotubes/silver-coated nylon 6 as microwave absorber. *Chem. Eng. J.* **2025**, *507*, 160188.
39 Cai, Z. Q.; Hao, X. D.; Sun, X. B.; Du, P. H.; Liu, W.; Fu, J. Highly active WO_3@anatase-SiO_2 aerogel for solar-light-driven phenanthrene degradation: Mechanism insight and toxicity assessment. *Water Res.* **2019**, *162*, 369–382.
40 Yang, Z.; Liu, H. J.; Zhao, J. Y.; Wang, C.; Li, H. T.; Wang, X. H.; Yang, Y.; Wu, H. X.; Gu, Z. P.; Li, Y. W. UV absorption enhanced polydopamine coating. *Mater. Horiz.* **2024**, *11*, 2438–2448.
41 Zou, Z. K.; Yang, P.; Li, X.; Liu, C.; Du, H.; Yang, Z.; Li, Y. W. Melanin-like polymers with boosted light absorption across the full spectrum for plant photoprotection. *Polymer* **2026**, *343*, 129397.

https://doi.org/10.1007/s10118-026-3690-x